

Enhancing nitrogen solubility in GaAs and InAs by surface kinetics: An *ab initio* study

Hazem Abu-Farsakh and Jörg Neugebauer

Max-Planck-Institut für Eisenforschung GmbH, Max-Planck-Straße 1, 40237 Düsseldorf, Germany
and Universität Paderborn, Warburger Straße 100, 33098 Paderborn, Germany

(Received 19 September 2008; revised manuscript received 17 February 2009; published 14 April 2009)

Nitrogen solubility at GaAs and InAs (001) surfaces has been studied employing density-functional theory calculations. The effect of the surface reconstruction and the reconstruction-induced surface strain on N solubility was analyzed in detail, considering the various surface layers and sites. The stability phase diagrams for the considered systems were constructed, and based on them an estimate of the N concentration has been deduced for the thermodynamically accessible and relevant range of chemical potentials in the various surface layers and at a typical growth temperature of 500 °C. Our results show that the solubility of N at the surface is unexpectedly rich and a complex function of the surface reconstructions. We discuss the possible N incorporation mechanisms and the conditions that allow for an enhanced solubility which can be in GaAs up to five orders of magnitude higher than the equilibrium bulk solubility. In addition, we find that the solubility of N at the GaAs(001) surface is one to four orders of magnitude higher than that at the InAs(001) surface.

DOI: 10.1103/PhysRevB.79.155311

PACS number(s): 64.75.Bc, 68.35.Md

I. INTRODUCTION

Ternary $\text{GaAs}_{1-x}\text{N}_x$ alloys with low N content have recently sparked a considerable theoretical and experimental interests due to their unique physical properties. Unlike conventional ternary III-V alloys, the incorporation of a few percent of N in GaAs results in a large band-gap bowing,¹⁻³ making this material system interesting for applications such as infrared laser diodes operating in the 1.3–1.6 μm region relevant for optical data transmission. A specific problem for practical applications is the very low equilibrium bulk solubility of N in GaAs, which was estimated to be $\sim 10^{-7}\%$ at $T=1000$ K.⁴ The origin of the low solubility is the large difference in bond length between Ga-N and Ga-As of more than 20%.² Therefore, substituting N on an As site causes considerable tensile strain around the N atom.

An interesting approach to overcome the limited bulk equilibrium solubility is to employ surface kinetics. It was demonstrated that the solubility of impurities is enhanced near surfaces because of strain relief and surface reconstruction.⁵ For example, based on theoretical studies it has been proposed that the solubility of N can be dramatically enhanced by 5 orders of magnitude in the subsurface region of the GaAs(001) surface at 1000 K as a result of the surface strain induced by As dimers at the surface.⁶ There is a lot of interest to employ such a mechanism in epitaxy and to increase the N solubility by kinetically freezing in the surface concentration. A qualitative description of the relevant mechanisms is given in Fig. 1. It schematically shows the formation energy of substituting a N atom at a reconstructed GaAs(001) surface as a function of the surface layer it gets incorporated. The dashed horizontal lines represent the thermal threshold energies $E_{\text{th}} = k_B T \ln \frac{\Gamma_0}{\Gamma}$ with k_B as the Boltzmann constant, T as the growth temperature, and Γ_0/Γ as the prefactor/rate for a specific diffusion event. Assuming a common attempt frequency of 10^{13} s^{-1} and that the diffusing atom can be regarded as mobile if the hopping rate between surface layers is $\Gamma \approx 1 \text{ s}^{-1}$ this energy becomes $E_{\text{th}} \approx 30k_B T$. The figure shows the threshold diffusion ener-

gies $E_{\text{th}1}, \dots, E_{\text{th}3}$ corresponding to a set of temperatures T_1, \dots, T_3 with $T_1 > T_2 > T_3$. If the threshold energy is above the corresponding left or right barrier the adatom is able to jump over it at a rate comparable to molecular-beam epitaxy (MBE) growth. If such a vertical transport is enabled the corresponding surface layers can equilibrate. From Fig. 1 there are two main aspects to note: (i) in general, the formation energy to incorporate or substitute the adatom will be higher (less favorable) in the bulk than at the surface layers

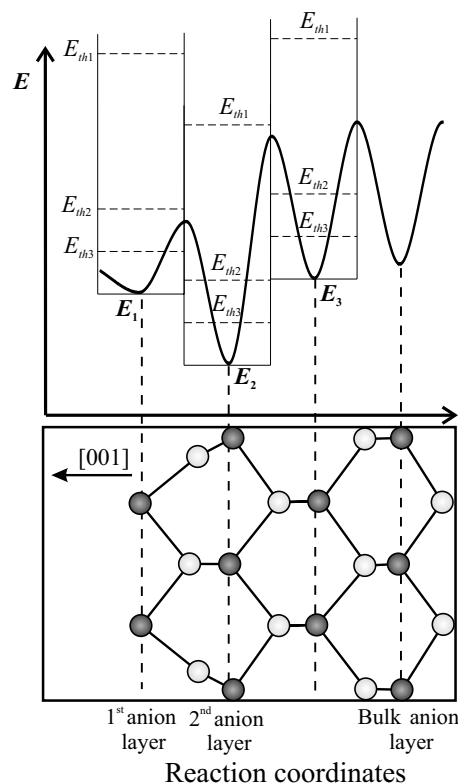


FIG. 1. Schematic representation of the formation energy of substitutional incorporation of a N atom at GaAs(001) surface (see text).

and (ii) it can be lowest (most favorable) in the subsurface layer (second anion layer) as a consequence of the surface reconstruction. If growth takes place under complete thermodynamic equilibrium (e.g., at temperature T_1 corresponding to E_{th1}) then the resulting N concentration will be very low. Lowering the growth temperature (e.g., at T_2 corresponding to E_{th2}) allows the subsurface (second anion layer) incorporation while preventing equilibration with the bulk. For this case, the solubility in the subsurface layer can be frozen in as the crystal grows, which leads to an enhanced solubility of N. During growth, an additional layer will be added to the surface, the second layer becomes the third, and the energy of the N atom changes from E_2 to E_3 . Since for this site the barrier from E_3 to E_2 is higher than the threshold energy E_{th2} the N atom is prevented from going into its ground state in E_2 . The nitrogen concentration is thus given by the subsurface energy E_2 rather than by the bulk energy. At even lower temperatures (e.g., at T_3 corresponding to E_{th3}) equilibration is restricted to the top surface layer, i.e., the resulting bulk concentration is solely determined by the solubility in the first surface layer. Therefore, the highest N solubility can be achieved if N incorporation in the subsurface region is operational, i.e., at a thermal energy which is sufficient to overcome the barrier from E_1 to E_2 but too low to overcome the barrier from E_2 to E_1 and from E_3 to E_2 .

In order to identify suitable growth conditions, where surface kinetics prevails over bulk thermodynamics, it is crucial to understand or quantify (i) the formation energies needed to substitute nitrogen in the various layers and for all relevant surface reconstructions and (ii) the kinetic barriers.

A second possible approach to enhance solubility is the growth of quaternary alloys. These alloys contain in addition to the nitrogen atom a larger sized atom, which allows a partial cancellation of the large tensile strain fields present in the ternary $\text{GaAs}_{1-x}\text{N}_x$ system around the small N atom. Moreover, going from ternaries to quaternaries provides an additional handle to tune the physical properties. This has initiated the growth and characterization of $\text{In}_x\text{Ga}_{1-x}\text{As}_{1-y}\text{N}_y$ quaternary alloys for practical applications including infrared laser diodes and solar cells.⁷⁻⁹ Furthermore, the ternary $\text{InAs}_{1-x}\text{N}_x$ material system is by itself promising for mid-infrared 2–5 μm devices.^{10,11} The incorporation of In in $\text{GaAs}_{1-x}\text{N}_x$, which has the same valency as N, allows for the compensation of the tensile strain induced by N and therefore allows the alloy to be lattice matched to GaAs. A crucial issue in quaternary alloys is that the macroscopic composition of the elements does not uniquely determine their spatial arrangement, which affects strongly their physical properties. Therefore, there are difficulties in realizing this material system for applications: compositional fluctuations and a preferred formation of Ga-N and In-As bonds have been reported.¹²⁻¹⁴ Recently, it has been shown that a repulsive interaction between In and N at the uppermost surface layer causes an In-N anticorrelation behavior.¹⁵ This finding suggests that the solubility of N is reduced in In-rich regions of the alloy. Therefore, in this study we considered also the solubility of N in and at $\text{InAs}(001)$ surfaces.

The aim of the present paper is to determine the solubility of N in GaAs and InAs by taking into account the various incorporation mechanisms (surface, subsurface, and bulk)

and all relevant surface reconstructions. The focus will be on the (001) surfaces and typical MBE growth conditions will be assumed.

II. METHODOLOGY

A. Computational details

The equilibrium geometries and the formation energies for the adatom incorporation were calculated employing density-functional theory (DFT) within the plane-wave pseudopotential method as implemented in the *S/PHI/NX* code.¹⁶ The generalized gradient approximation (GGA) was used for exchange and correlation.¹⁷ Fully separable¹⁸ norm-conserving pseudopotentials of the Troullier-Martins type¹⁹ were used. A plane-wave cutoff energy of 40 Ry was found to give converged atomic geometries and surface energies. The surfaces were described by a repeated slab geometry consisting of eight atomic layers and a vacuum thickness equivalent to eight atomic layers. The backside of the slabs was passivated with an additional layer of pseudohydrogen atoms to ensure local charge neutrality. The uppermost six atomic layers were allowed to fully relax. An equivalent k -point sampling using a $4 \times 4 \times 4$ Monkhorst-Pack²⁰ mesh per orthorhombic unit cell for both bulk and surface systems was used. Lattice constants were optimized and found to be 5.73 Å for GaAs and 6.12 Å for InAs (experimental values are 5.65 and 6.03 Å, respectively).²¹ The calculations were performed in a single surface unit cell (2×4 or 4×2 reconstruction) for the slab calculations and in a 2×4 orthorhombic cell for the bulk calculations. Extensive convergence checks were performed for N substitutions in the energetically *most favorable* sites at three different surface reconstructions of the $\text{GaAs}(001)$ surface and in the bulk as well. The largest error in the formation energies is due to the size of the supercells employed here. Convergence checks showed this error to be less than 0.05 eV for the surface calculations and of about 0.1 eV for the bulk.²²

B. Surface and bulk thermodynamics

In order to determine the solubility of an impurity in a given structure the energy needed to incorporate or substitute it into that structure, i.e., its formation energy, is required. To determine the solubility of N in various surface reconstructions we define the formation energies relative to the reconstructed surface without adatom. For the replacement of an As by a N atom this can be written as

$$\Delta H_{\text{N}}^f = \Delta E^{\text{tot}} - \Delta n_{\text{Ga}}\mu_{\text{Ga}} - \Delta n_{\text{As}}\mu_{\text{As}} - \Delta n_{\text{N}}\mu_{\text{N}}, \quad (1)$$

where ΔE^{tot} is the total-energy difference between the system and the reference, Δn_{α} is the difference in the number of atoms of species α between the system and the reference, and μ_{α} is the chemical potential of species α . For GaAs to be thermodynamically stable it is required that $\mu_{\text{GaAs}} = \mu_{\text{Ga}} + \mu_{\text{As}}$ and thus Eq. (1) can be reduced to a function of two chemical potentials ($\mu_{\text{As}}, \mu_{\text{N}}$),

$$\Delta H_{\text{N}}^f = \Delta E^{\text{tot}} - \Delta n_{\text{Ga}}\mu_{\text{GaAs}} - (\Delta n_{\text{As}} - \Delta n_{\text{Ga}})\mu_{\text{As}} - \Delta n_{\text{N}}\mu_{\text{N}}. \quad (2)$$

TABLE I. Calculated formation enthalpies of all relevant bulk binaries and the binding energy of the N reservoir (N_2 molecules) compared to previous theoretical and experimental results.

	ΔH^f (eV)	
	Theory	Experiment
GaAs	-0.74 ^a	-0.74 ^b
InAs	-0.65 ^a	-0.61 ^b
GaN	-1.09, ^a -1.11 ^c	-1.15 ^b
InN	-0.31, ^a -0.31 ^c	-0.30 ^d
	Binding energy (eV)	
N_2	10.20, ^a 10.69 ^c	9.80 ^b

^aPresent work.

^bReference 23.

^cReference 24.

^dReference 25.

The formation of parasitic phases (As bulk and N_2 molecules) puts further restrictions on the choice of the chemical potentials; $\mu_{As} \leq \mu_{As}^{bulk}$ and $\mu_N \leq \mu_{N_2}$. Using these relations, the bounds the chemical potentials have to obey can be written as

$$\mu_{As}^{bulk} + \Delta H_{GaAs}^f \leq \mu_{As} \leq \mu_{As}^{bulk}, \quad (3)$$

$$\mu_N \leq \mu_{N_2}. \quad (4)$$

Here ΔH_{GaAs}^f is the heat of formation of GaAs bulk. The right-hand side of Eqs. (3) and (4) represent As-rich (Ga-poor) and N-rich conditions, respectively, while the left-hand side of Eq. (3) represents As-poor (Ga-rich) conditions. The same formalism applies in the case of InAs surfaces, replacing Ga with In. To calculate the formation energy of N into bulk the same formalism can be employed, using the host bulk as the reference system. The calculated formation energies for the related systems are listed in Table I, together with previous theoretical and experimental results. In all cases a good agreement is found.

III. RESULTS AND DISCUSSION

A. N solubility at GaAs(001) surface

1. Effect of local strain

To investigate N at surfaces we restrict our study to the well-known reconstructions of the clean GaAs(001) surface. Recent studies have reported that impurities can stabilize unusual surface reconstructions.^{26,27} In the case of dilute N concentrations which is considered here it is unlikely that N changes the surface reconstruction. This is supported by experimental results^{28,29} which also report that only by going to high N concentrations and high growth temperatures the surface transforms into a 3×3 reconstruction. However, when growing GaAsN or InAsN alloy it is crucial to avoid these

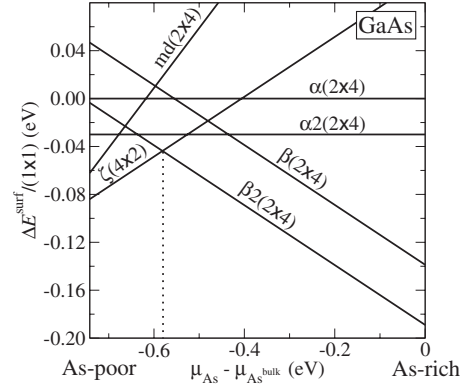


FIG. 2. Calculated phase diagram of the clean GaAs(001) surface. The dotted line indicates the phase boundary between $\beta 2(2 \times 4)$ and $\zeta(4 \times 2)$ reconstructions.

surface reconstructions since they act as precursors to the formation of parasitic phases such as GaN or InN and result in a deterioration of the material quality.

As a first step we calculated the formation energies [Eq. (2) with $\Delta n_N = 0$] of the various bare GaAs(001) surface reconstructions. Based on these results the corresponding surface phase diagram was constructed. The bounds of the As chemical potential were determined from Eq. (3). As reference system we chose the $\alpha(2 \times 4)$ surface. The computed phase diagram is shown in Fig. 2. It agrees well with previous theoretical and experimental results.^{30,31} We point out that the $c(4 \times 4)$ reconstruction was not considered here since this reconstruction is thermodynamically stable only under extreme As-rich conditions, i.e., under conditions which are not suitable for N incorporation. Based on the calculated phase diagram we selected the three most stable or metastable reconstructions relevant for N incorporation in the region between As-moderate and As-poor conditions. These are the $\beta 2(2 \times 4)$, the $\alpha 2(2 \times 4)$, and the $\zeta(4 \times 2)$ reconstructions. Schematic representations of the atomic structure of these reconstructions are shown in Fig. 3.

In the next step we replaced an As atom with a N atom in one of the surface layers. Symmetry nonequivalent sites in the first and second anion layers have been considered. The labeling of the sites is shown in Fig. 3; the a sites are in the a layer (first anion layer) and the c sites are in the c layer (second anion layer).

Since the main focus of the present study is the surface enhanced solubility we will discuss in the following the segregation energy rather than the total formation energy. The segregation energy is defined as

$$E_{seg} = \Delta H_{Nsurf}^f - \Delta H_{Nbulk}^f = \Delta E_{Nsurf}^{tot} - \Delta E_{Nbulk}^{tot}. \quad (5)$$

Here, ΔH_{Nsurf}^f and H_{Nbulk}^f are the formation energies of N substitution at a surface site and in the bulk, respectively. Note that the latter equality follows directly from Eq. (2). According to this definition, a negative segregation energy indicates that N is more stable at the surface than in the bulk, i.e., surface segregation will occur, while a positive energy implies that surface segregation is suppressed.

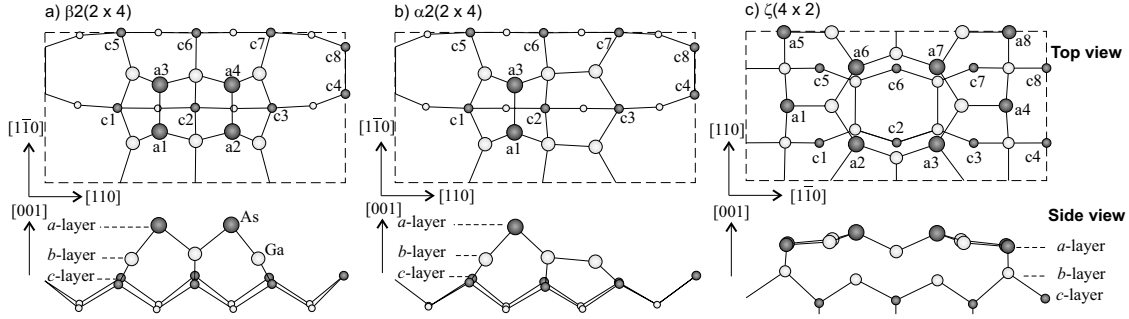


FIG. 3. Schematic representation of the selected GaAs(001) surface reconstructions showing top and side views. The reconstructions are (a) $\beta 2(2 \times 4)$, (b) $\alpha 2(2 \times 4)$, and (c) $\zeta(4 \times 2)$. Black (white) spheres represent As (Ga) atoms. Larger spheres indicate atoms in the upper surface layers (a and b layers). The labels give the notation for the N sites used in the text.

Let us first discuss the results for the $\beta 2(2 \times 4)$ reconstruction. This reconstruction is of specific importance because of its stability over a wide range of chemical potentials (see Fig. 2 and Ref. 30). The calculated segregation energies are summarized in Table II (fourth column). The results clearly show that the N segregation energy strongly depends on the specific surface site. The lowest-energy configuration for N is in the second anion layer (c layer) at the central position below two As dimers (i.e., at position $c2$). The strong energetic preference of this site agrees with results reported in previous studies^{32,33} A similar site for a 2×1 reconstruction was also reported to be energetically preferable.⁶ In the first anion layer, the energetically preferred sites are $a3/a4$. However, compared to the most favorable $c2$ site their energy is higher by 0.55 eV. The segregation energies at the other first anion layer sites ($a1/a2$) are similar because they are almost equivalent to the $a3/a4$ sites [see Fig. 3(a)].

An interesting observation is that the segregation energy for a substitution in the second anion layer is strongly site dependent. For example, going from the $c2$ site along the $[1\bar{1}0]$ direction to the $c6$ site the segregation energy increases by almost 1.7 eV, despite the fact that the N atom is fully coordinated in both sites. This clearly indicates that local strain, caused by the surface reconstructions in the top surface layer, plays a major role. For example, the dimer

TABLE II. N segregation energies at the $\beta 2(2 \times 4)$ reconstructed GaAs(001) surface for the first and second anion layers. The last column shows the averaged segregation energies of each two neighboring N substitutional sites in the $[1\bar{1}0]$ direction. All energies are in eV.

Anion layer	N site	Coordination	E_{seg}	$\overline{E}_{\text{seg}}$
First	$a1, a2$	3	-0.12	
	$a3, a4$	3	-0.13	
Second	$c1, c3$	4	-0.49	
	$c5, c7$	4	0.70	0.11
	$c2$	4	-0.68	
	$c6$	4	1.00	0.16
	$c4$	3	0.13	
	$c8$	3	0.25	

contraction^{34–37} of an As dimer induces a compressive strain in the subsurface layer bonds which are directly below it and a tensile strain in the neighboring bonds in the $[1\bar{1}0]$ direction, i.e., the $c2$ site is under compressive strain while the $c6$ site is under tensile strain [Fig. 3(a)]. Incorporating a N atom at the $c2$ site partially releases the compressive strain, while incorporating a N at the neighboring site $c6$ further increases the tensile strain. In general, the As dimers in the first layer induce compressive strain on the atomic sites directly below them ($c1, c2,$ and $c6$) and tensile strain on the neighboring atomic sites ($c5, c6,$ and $c7$). In order to verify that the local compressive or tensile strain induced is the main origin for the strong variations in the segregation energies, we list in Table II (last column) the average segregation energy for each pair of sites along the $[1\bar{1}0]$ axis (i.e., parallel to the dimer bonds). To avoid chemical contributions only fully coordinated c layer sites are considered. We find that the average segregation energies are energetically almost degenerate within 0.05 eV, implying that indeed local strain effects cause the large energy differences between the individual sites.

Now let us consider the case of the $\alpha 2(2 \times 4)$ reconstruction. This structure is similar to the $\beta 2(2 \times 4)$; the main difference is a missing As dimer at the top surface layer [see Figs. 3(a) and 3(b)], making this structure less symmetric. The resulting segregation energies are listed in Table III. Also for this surface reconstruction the N segregation energy strongly depends on the specific surface site. The lowest N segregation energy is again for the $c2$ site being even lower in energy than for the $c2$ site in the $\beta 2(2 \times 4)$ reconstruction. We note that the N segregation energy for the $c3$ site is higher than that for the $c1$ site because of the missing As dimer above $c3$. The averaged segregation energy is also shown in the last column for each pair of sites along the $[1\bar{1}0]$ direction for the fully coordinated c -layer sites. The situation for the averaged segregation energies is more complicated than in the case of the $\beta 2(2 \times 4)$ and cannot be explained solely in terms of a simple elastic picture. The reason is that the chemical environment of the various sites is much more different than on $\beta 2(2 \times 4)$. Nevertheless, the effect of the local strain is still visible; the difference between the average segregation energies is significantly lower than the difference between the individual segregation energies.

TABLE III. Segregation energies (eV) of all N substitutions in the first and second anion layers of the $\alpha 2(2 \times 4)$ reconstructed GaAs(001) surface. The last column shows the averaged segregation energies of each two neighboring N substitutional sites in the $[1\bar{1}0]$ direction.

Anion layer	N site	Coordination	E_{seg}	$\overline{E}_{\text{seg}}$
First	$a1$	3	0.13	
	$a3$	3	0.12	
Second	$c1$	4	-0.16	
	$c5$	4	0.68	0.26
	$c2$	4	-1.01	
	$c6$	4	0.05	-0.48
	$c3$	4	-0.01	
	$c7$	4	0.34	0.16
	$c4$	3	0.24	
	$c8$	3	0.30	

Finally we show the results for the $\zeta(4 \times 2)$ reconstruction. This structure is geometrically rather complex and structurally very different from the former 2×4 reconstructions (see Fig. 3). The resulting segregation energies are summarized in Table IV. The averaged segregation energy is also shown in the last column for each two neighboring sites in the c layer as discussed previously. As the results show, the elastic picture no longer holds since the bonding between the top surface layer and the lower-lying layers is extremely inhomogeneous [see Fig. 3(c), bottom].

2. N stability phase diagrams

In order to determine the N solubility for the various surface reconstructions we construct the surface phase diagrams of N at GaAs and InAs(001) surfaces as function of the specific growth conditions (chemical potentials). The calculation of the phase diagrams is done according to the following steps: (i) first, we calculate the surface phase diagrams of the *clean* surface and identify the stable reconstructions and their region of thermodynamic stability; (ii) then, following the procedure described in Sec. III A 1 we identify for each re-

TABLE IV. Segregation energies (eV) of all N substitutions in the first and second anion layers of the $\zeta(4 \times 2)$ reconstructed GaAs(001) surface. The last column shows the averaged formation energies of each two neighboring N substitutional sites in the $[110]$ direction. The coordination number between parentheses is the original coordination number of the As atom at that site.

Anion layer	N site	Coordination	E_{seg}	$\overline{E}_{\text{seg}}$
First	$a1, a4$	3	0.01	
	$a5, a8$	3	-0.23	
	$a2, a3, a6, a7$	4(3)	-0.34	
Second	$c1, c3, c5, c7$	4	-0.39	-0.39
	$c2, c6$	4	0.24	0.24
	$c4, c8$	4	0.45	0.45

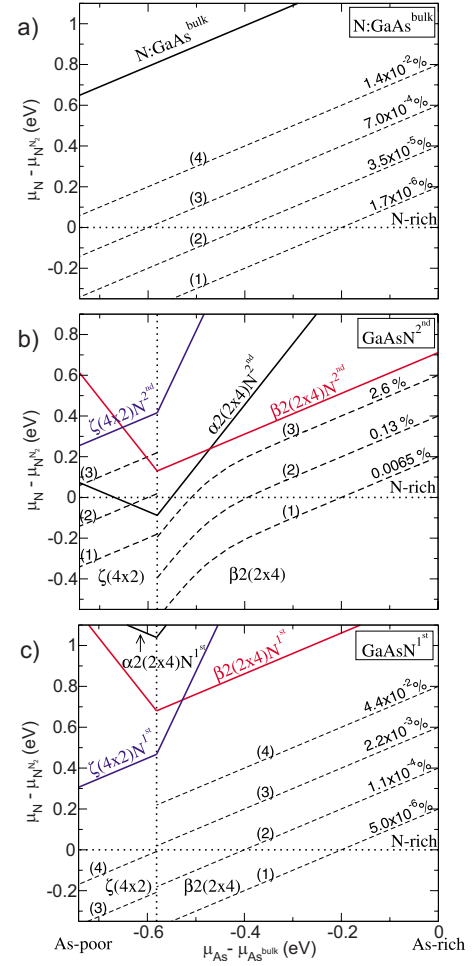


FIG. 4. (Color online) Solid lines: stability phase diagram of N in (a) GaAs bulk, (b) second anion layer, and (c) first anion layer of the GaAs(001) surface reconstructions. Dashed lines: contour lines of constant N concentration at $T=500$ °C. The dotted vertical line indicates the phase boundary between the $\beta 2(2 \times 4)$ and $\zeta(4 \times 2)$ reconstructions.

construction and in each layer the energetically most preferable site for N substitution; (iii) using the most favorable N substitution and Eq. (2) we calculate for each reconstruction and in each layer the formation energy of the N substitution as a function of growth conditions, relative to the clean surface stable at the corresponding As chemical potential; and (iv) finally we determine the thermodynamically stable regions for N substitution (defined by μ_{As} and μ_{N}), i.e., the growth window where the N substituted surfaces become more stable than the clean surfaces (i.e., $\Delta H_{\text{N}}^f \leq 0$). This is conventionally represented in a two-dimensional plot with μ_{As} and μ_{N} as independent variables.

The complete phase diagrams are shown in Fig. 4 for N incorporation (a) in bulk, (b) in the second anion surface layer (denoted with the adjunct $\text{N}^{2\text{nd}}$), and (c) in the first anion surface layer (denoted with the adjunct $\text{N}^{1\text{st}}$). The region where the corresponding N-rich surface becomes stable is marked by a solid line. A feature which may be a bit unusual is that our surface diagrams include also regions outside the thermodynamically allowed region. Specifically,

structures are included which are thermodynamically unstable against the decomposition into N_2 molecules. As will be later shown this is highly useful to discuss and derive surface solubility and to take into account kinetic growth aspects. From the phase diagrams we can directly conclude that:

- (i) Surfaces dramatically reduce the energy needed to substitute N in GaAs.
- (ii) The second anion layer is energetically more attractive for N atoms than the first.

(iii) In a small thermodynamic window the formation of a GaAsN surface alloy becomes exothermic [formation of the $\alpha 2(2 \times 4)$ reconstruction with N in the second anion layer].

(iv) N is very reactive and may change the surface reconstruction for fixed Ga/As ratio (fixed μ_{As}).

The last issue (iv) becomes evident when inspecting, e.g., Fig. 4(b) where under modest As-rich conditions the $\alpha 2(2 \times 4)$ reconstruction becomes stable is *not* a stable one in the bare GaAs surface phase diagram (Fig. 2). Another example is shown in Fig. 4(c) where the $\zeta(4 \times 2)$ reconstruction becomes stable in a region where in the absence of N only the $\beta 2(2 \times 4)$ reconstruction is observed. Furthermore, from the phase diagram (Fig. 4) the incorporation of N is strongly enhanced when going from As-rich to Ga-rich conditions. This by itself is not unexpected since to replace an As with a N atom the former has to be lowest in its chemical potential where the energy gain is largest for Ga-rich conditions. What is more interesting is that at the surfaces this behavior is not linear like in the bulk but shows different slopes and even a nonmonotonous behavior. This indicates that the maximal N solubility is not necessarily achieved under extreme As-poor conditions as one might naively expect from the pure bulk behavior.

3. N solubility and concentration: Method

Based on the calculated phase diagrams and employing Boltzmann statistics, the concentration of N in the dilute limit can be determined as a function of the specific growth conditions (μ_{As} , μ_N , and T). As shown in Fig. 4, the N substitution energy depends strongly on the surface layer as well as on the specific site. The maximal solubility which can be achieved thus depends on the surface kinetics, which determines the kinetically accessible layers (see Fig. 1). In order to gain insight how different kinetics might affect solubility we consider the *layer-resolved* N solubility, i.e., the N solubility at each individual surface layer. The equilibrium concentration of N in the l th surface layer is given by

$$c_l^\sigma = \sum_i c_{l,i}^{\sigma,0} e^{-\Delta H_{l,i}^\sigma / k_B T}. \quad (6)$$

Here, the superscript σ specifies the surface reconstruction. The index i runs over the nonequivalent substitutional sites in that layer, $c_{l,i}^{\sigma,0} = \frac{n_i^\sigma}{n_{\text{bulk}}}$ is the concentration of that site, where n_i^σ is the number of equivalent substitutional sites in that layer and n_{bulk} is the number of all substitutional sites in a bulk (001) layer of an equivalent area, and $\Delta H_{l,i}^\sigma$ is calculated according to Eq. (2) for given chemical potentials (μ_{As} and μ_N). In the present study it turned out that in most layers a

single set of symmetry equivalent sites dominates since these sites have a much lower energy than all others. In this case, to a very good approximation, Eq. (6) can be simplified to

$$c_l^\sigma \approx c_{l,i_{\min}}^{\sigma,0} e^{-\Delta H_{l,i_{\min}}^\sigma / k_B T}. \quad (7)$$

Here the index i_{\min} gives the energetically preferred structure at each layer.

An important issue which needs specific attention is that substituting N in the surface may destabilize the original surface reconstruction and stabilize a new one, i.e., incorporating N may induce a local phase transition. A prominent example is the stabilization of the $\alpha 2(2 \times 4)$ reconstruction under modest to poor As chemical-potential conditions as clear from Fig. 4(b). This reconstruction is in the absence of N unstable against the formation of the $\beta 2(2 \times 4)$ surface at modest As chemical potential and against the formation of a $\zeta(4 \times 2)$ reconstruction at poor As chemical potential. Also, the presence of N significantly affects the surface phase diagram and, e.g., shifts the transition from the $\zeta(4 \times 2)$ to the $\beta 2(2 \times 4)$ phase toward more As-rich conditions [Fig. 4(c)]. The fact that N can be incorporated both in the original surface reconstruction and in a new N-induced structure is very different from the conventional impurity picture where a fixed host (and thus reference system) is assumed. Calculating the net N solubility at the surface is therefore no longer given by a simple Boltzmann statistics. Various phases that can form at the surface and are induced by N itself contribute to the net N concentration. It is therefore essential to know what are the phases that contribute to the net N concentration under certain conditions and what are their contributions.

The mechanism that controls the possibility for a N-induced phase transition is the interface energy between the N-stabilized reconstruction and the clean surface reconstruction. In order to quantify the N concentration we assume two possible cases in the phase diagram. (i) The first case is when the interface energy is high. In this case the local phase transition occurs only if the N atoms are incorporated in neighboring cells and form a cluster large enough to form a stable nucleus. Such agglomeration of N atoms is highly prohibitive due to configuration entropy and can be excluded in the dilute concentration limit relevant for the N incorporation. Therefore, the N atoms will be incorporated only in the originally stable phase without inducing a phase transition. The other reconstructions hence will not contribute to the total N concentration and the concentration can be directly calculated from Eq. (6). An example for this case is in the As-poor region in Fig. 4(b), where the formation energies of N in $\alpha 2(2 \times 4)$ and $\beta 2(2 \times 4)$ are lower than in the stable $\zeta(4 \times 2)$. However, $\alpha 2(2 \times 4)$ [or $\beta 2(2 \times 4)$] and $\zeta(4 \times 2)$ are structurally very different and thus the interface energy is expected to be $\gg k_B T$. Hence the N atoms will not induce a phase transition and only the formation energy of N in the $\zeta(4 \times 2)$ reconstruction will determine its concentration. (ii) The second possible case is when the interface energy is negligible. Here a N-induced local phase transition is possible and the N atoms will be statistically distributed in the two phases. An example for this case is in Fig. 4(b) under modest As conditions where the formation energy of N sub-

stitution in $\alpha 2(2 \times 4)$ is lower than in the stable $\beta 2(2 \times 4)$. Note that the two reconstructions are structurally very similar and can be transformed into each other by adding or removing a single As dimer [see Fig. 3]. Explicit *ab initio* calculations showed that this is well justified. For example, building a cell of alternating $\alpha 2(2 \times 4)$ and $\beta 2(2 \times 4)$ reconstructions along the $[1\bar{1}0]$ costs less than 11 meV per boundary which is smaller than the total formation energy. Neglecting this small interface energy the total concentration of N becomes simply the sum of the N concentrations in each phase,

$$c_l = \sum_{\sigma} c_l^{\sigma}. \quad (8)$$

The index σ goes only over the *relevant* reconstructions, i.e., only the reconstructions which have a negligible interaction energy with the stable clean reconstruction for the given As chemical potential are considered. The independent concentrations c_l^{σ} are calculated according to Eq. (6) with the stable clean reconstruction at the specific μ_{As} as the reference surface for calculating the formation energies ΔH_i^f . Note that Eq. (8) principally allows N atoms to occupy the same site more than once. Therefore, this approximation is valid only in the dilute concentration limit. Preliminary Monte Carlo simulations³⁸ which go beyond these approximations have provided identical results. For bulk, the equilibrium N concentration [Eq. (6)] simplifies to

$$c_{\text{bulk}} = e^{-\Delta H_{\text{bulk}}^f/k_B T}. \quad (9)$$

Here ΔH_{bulk}^f is the formation energy of N incorporation in the bulk relative to the clean bulk system. Using this approach, lines with constant N concentration have been calculated and included in Fig. 4. A growth temperature of 500 °C has been assumed.

4. N solubility and concentration: Results

Let us start by discussing the solubility limit in GaAs bulk. From the concentration lines in Fig. 4(a) it is clear that the maximum solubility limit which can be achieved in GaAs bulk under thermodynamic equilibrium is very low. It is on the order of $\sim 10^{-3}\%$ under extreme N- and As-poor conditions.

At the second anion surface layer (*c* layer), a set of three selected N-concentration lines [obtained using Eq. (8)] are shown in the phase diagram in Fig. 4(b). The concentration lines were chosen, so that they partially coincide (at the As-rich limit) with the bulk concentration lines to allow for a direct comparison. We note the close relation between the concentration lines and the stability lines (the solid lines) of the corresponding phases. The concentration lines indicate a general increase in N solubility with decreasing As chemical potential, except at the discontinuity associated with the phase transition between the $\beta 2(2 \times 4)$ and the $\zeta(4 \times 2)$ reconstructions. This discontinuity causes an abrupt decrease in the N solubility. These results highlight again the large effect the specific surface reconstruction has on the N solubility. The optimal As chemical potential (μ_{As}) to achieve maximal N concentrations is just before the phase transition

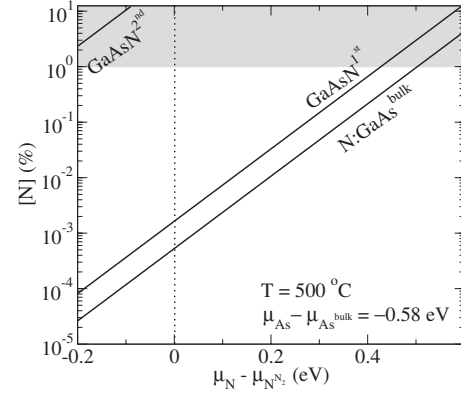


FIG. 5. Calculated N concentration in GaAs as a function of N chemical potential at $T=500$ °C and $\mu_{\text{As}} - \mu_{\text{As,bulk}} = -0.58$ eV. The different lines represent the different N incorporation mechanisms. The shaded region represent the experimentally relevant range of N concentrations (Refs. 29 and 39–41).

from $\beta 2(2 \times 4)$ to $\zeta(4 \times 2)$, i.e., at $\mu_{\text{As}} - \mu_{\text{As,bulk}} = -0.58$ eV (Fig. 4). We note that under these conditions it is possible to achieve N concentrations as high as 12.5%. Comparing this solubility to that in the bulk, an increase by about 3–5 orders of magnitude is found.

In the next step we consider the case of N incorporation at the top surface layer (i.e., in the first anion layer). The corresponding concentration lines are included in Fig. 4(c). The concentration lines are again chosen to coincide with those in Figs. 4(a) and 4(b) at the As-rich region to allow for a direct comparison between the three cases. Since the $\zeta(4 \times 2)$ reconstruction is usually not suitable for growing GaAs, the optimal As chemical potential (μ_{As}) to achieve high N concentrations is equivalent to that in the case of the second anion layer substitution, i.e., at $\mu_{\text{As}} - \mu_{\text{As,bulk}} = -0.58$ eV.

Comparing the case of incorporation into the first anion layer with that into the second anion layer, we note that the N solubility in the first anion layer is lower by up to 4 orders of magnitude (under moderate As conditions). This finding is a direct consequence of the reconstruction-induced strain in the subsurface layers as discussed in Sec. III A 1. Comparing to the bulk solubility, the maximal N concentration in the first anion layer incorporation is still higher by $\lesssim 1-2$ orders of magnitude.

In order to summarize the main results we show in Fig. 5 the maximal N solubility as function of the N chemical potential for optimal As chemical-potential conditions ($\mu_{\text{As}} - \mu_{\text{As,bulk}} = -0.58$ eV) and for the three different N incorporation mechanisms: surface, subsurface, and bulk.

5. Discussion

A consequence of the above results is that N solubility exhibits a complex behavior and depends strongly on the active incorporation mechanism. The first mechanism (bulk incorporation) is active under complete thermodynamic equilibrium conditions, i.e., all surface layers and the bulk are in thermodynamic equilibrium with the chemical reservoirs in the growth chamber, and an unrestricted exchange of all atoms is allowed. As our results show, this mechanism leads to

a very poor N solubility [$\sim 10^{-3}\%$ N; see Fig. 4(a) under As-poor and N-rich conditions] and cannot explain the experimentally achieved N solubility.

The second mechanism is N incorporation in the subsurface region of GaAs(001), i.e., the second anion layer is at thermodynamic equilibrium with the upper layers but not in equilibrium with the bulk. For this scenario, a N concentration as high as 12.5% can be achieved at moderate As- and N-rich conditions (Fig. 5). Recent combined theoretical and experimental studies¹⁵ showed that this mechanism is not active under typical growth conditions. This finding is also supported by preliminary theoretical studies of the kinetic barriers which show that the barrier for a N atom to go from the top surface to subsurface cannot be overcome at a temperature of 500 °C.³⁸ Therefore, this incorporation mechanism is not active and will be excluded from the further discussion.

The last mechanism is the incorporation of N in the top surface layer; i.e., thermodynamic equilibrium is restricted solely to the uppermost surface layer. Although this mechanism leads to a higher N solubility than the bulk equilibrium solubility, it is still well below the N concentrations which are routinely achieved in MBE experiments. This can be seen in Fig. 5 by the discrepancy between the gray shaded area and the first layer concentration at $\mu_N=0$ (dotted line). Zero chemical potential means here that the surface is in thermodynamic equilibrium with N_2 molecules in the gas phase. To achieve such an equilibrium, excess N atoms at the surface must be able to form N_2 molecules without kinetic limitations. In a realistic growth environment, a thermodynamic equilibrium with the N_2 gas will be hard or impossible to realize. First, in MBE growth a N plasma source is usually used, which provides excited N_2 molecules (N_2^*) and/or atomic N. These activated species correspond to a much higher N chemical potential than that of the N_2 molecules. Experimentally, it has been shown that the characteristic vibrational temperature for the excited N_2 molecules in a N plasma source is $>10^4$ K (i.e., corresponding to a thermal energy of ~ 0.86 eV) and the dissociation fraction of the N_2 molecules can be up to 70%.⁴² Second, a spontaneous formation of N_2 molecules at the surface can be achieved only if the N atoms are sufficiently mobile and provided that the repulsive interaction between N atoms is sufficiently small, so that it can be overcome at characteristic growth temperatures. Both mechanisms indicate that under typical MBE growth conditions the actual N chemical potential at the surface can be shifted by a few tenths of an eV toward higher energies.

Another potential upper limit of the N chemical potential is the formation of parasitic GaN. Earlier theoretical studies calculating the solubility of N in GaAs have assumed the chemical-potential reservoir to be that of bulk GaN.⁶ Zhang and Wei³³ then proposed that μ_N can be further increased, since a relaxed GaN phase can form only after the formation of a N-rich cluster of critical size for dislocation formation, which in turn can form only after a spontaneous formation of a N-rich layer at the GaAs surface. The upper limit for μ_N was raised accordingly, i.e., to the point where the formation energy of N substitution at the surface equals to zero. In order to explain this and based on our results (Fig. 4) we

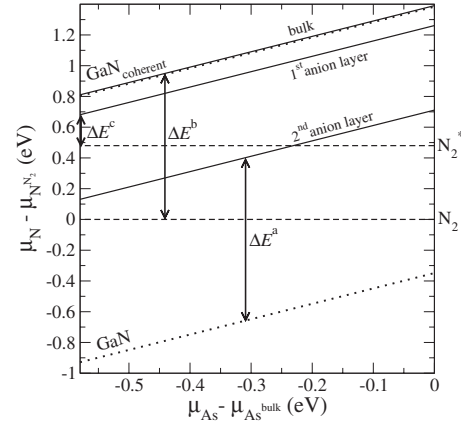


FIG. 6. Stability phase diagram of N in bulk GaAs and in the surface layers of the $\beta 2(2 \times 4)$ reconstruction of GaAs(001) (solid lines). The dotted lines define the stability regions for bulk GaN and the coherent bulk GaN (at the lateral lattice constant of GaAs; see text). Note that the latter line almost coincides with the stability line of N in bulk GaAs. The dashed lines indicate the chemical potential of N_2 and excited N_2 molecules (N_2^*). The arrows indicate the mechanism and formation energy used to calculate N solubility in Ref. 6 (ΔE^a), Ref. 33 (ΔE^b), and present work (ΔE^c). μ_{As} is restricted to the relevant region for N incorporation, i.e., to the region where the $\beta 2(2 \times 4)$ reconstructed surface is stable.

show in Fig. 6 the stability phase diagram for N substitution in bulk GaAs and in the surface layers of the $\beta 2(2 \times 4)$ reconstruction, showing also the stability regions for bulk GaN, the coherent GaN phase (at the lateral GaAs lattice constant), and of the N_2 molecules. It becomes clear that the formation of a coherent GaN layer or precipitate is unfavorable. Only when assuming strongly nonequilibrium conditions with $\mu_N \gg \mu_{N_2}$ sufficiently high N concentrations may be reached to form a coherent GaN cluster. Only if this cluster exceeds a critical size or thickness a fully relaxed GaN precipitate can form. Therefore, under typical MBE conditions, we expect that μ_N can be increased beyond μ_{N_2} without the formation of the relaxed GaN phase. Following this assumption and based on our results in the region where the $\beta 2(2 \times 4)$ reconstruction is stable (relevant for MBE growth), μ_N can be increased by 0.68 eV above μ_{N_2} before spontaneously forming a coherent GaN layer. In contrast, to incorporate about 2% of N (assuming the first anion layer incorporation mechanism) it is sufficient to increase μ_N by 0.48 eV above μ_{N_2} (indicated in Fig. 6 as a dashed line marked with N_2^*).

In previous studies, two incorporation mechanisms have been proposed to explain the high N concentration which can be realized in experiment and which is much higher than the bulk N solubility. While these models had an important impact to qualitatively gain insight into realistic dopant incorporation, the underlying surface models were rather approximate due to the limited computer resources available at that time. Based on the stability phase diagram summarized in Fig. 6 we are able to carefully re-examine these proposals and to identify the solubility for each of them. In the early work by Zhang and Zunger⁶ it has been assumed that N substitutes in the second anion surface layer, i.e., in our ter-

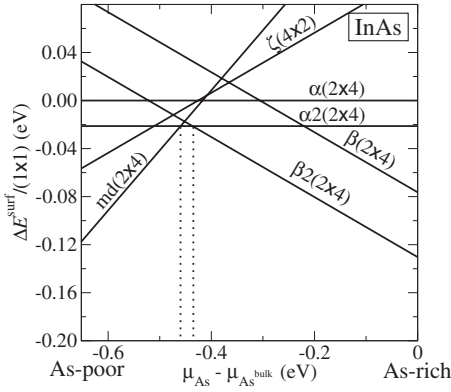


FIG. 7. Phase diagram of the clean InAs(001) surface. The dotted lines indicate the phase boundaries between $\beta 2(2 \times 4)$, $\alpha 2(2 \times 4)$, and $\text{md}(2 \times 4)$ reconstructions.

minology that the subsurface incorporation mechanism is active. Using the valance force field approach, a 2×1 reconstruction and GaN as the chemical-potential reservoir they obtained a substitution energy of $\Delta E=0.7$ eV. With $T=727$ °C and assuming three sites of this type per layer of the actual $\beta 2(2 \times 4)$ cell they calculated a concentration of $\sim 0.045\%$. Replacing the approximate 2×1 reconstruction with a realistic $\beta 2(2 \times 4)$ cell, the corresponding substitution energy increases slightly ($\Delta E^a=1.06$ eV in Fig. 6). For actual MBE growth conditions ($T=500$ °C) this translates into a N concentration of $\approx 10^{-6}\%$, i.e., too low to explain experiment. A second mechanism proposed by Zhang and Wei³³ assumes the third incorporation mechanism (bulk incorporation) to be the active mechanism. In that study the chemical-potential limits were extended to the point where the formation of N substitution at the top surface layer becomes stable. With this they obtained $\mu_{\text{N}}^{\text{max}}=0$ and $\mu_{\text{As}}^{\text{min}}=-0.44$ eV, and hence a substitution energy of $\Delta E=0.24$ eV. Using $T=650$ °C they calculated a N concentration of 4%. However, based on our calculations the first layer incorporation does not become stable in the thermodynamically allowed range. Using their values of the chemical-potential limits we get $\Delta E=0.95$ eV (indicated by ΔE^b in Fig. 6). This value can be reduced to 0.65 eV by going to more As-poor conditions. The large discrepancy is most likely related to using a reduced plane-wave cutoff energy of 25 Ry and local-density approximation (LDA) pseudopotentials. Using our data, this mechanism gives a N solubility of $\approx 0.006\%$ at $T=500$ °C, again too low to explain experiment. In contrast, assuming an incorporation in the first anion surface layer and an excited N_2 source, the lowest formation energy to incorporate N at the surface (indicated by ΔE^c in Fig. 6) gives solubilities in accordance with experiment.

B. N solubility at InAs(001) surfaces

We now determine the solubility of N at the InAs(001) surface by employing the same procedure as used for the GaAs(001) surface. In the first step the clean surface phase diagram has been calculated (Fig. 7). The phase diagram provides a set of low-energy reconstructions which we consider for N substitutions. These are the $\beta 2(2 \times 4)$,

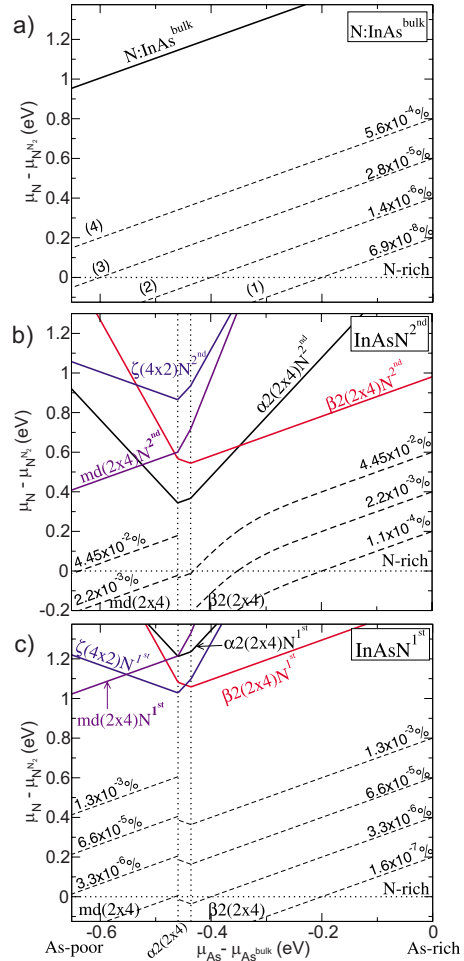


FIG. 8. (Color online) (a)–(c) Same as in Fig. 4 but for InAs. The dotted lines indicate the phase boundaries between $\beta 2(2 \times 4)$, $\alpha 2(2 \times 4)$, and $\text{md}(2 \times 4)$ reconstructions.

$\alpha 2(2 \times 4)$, mixed-dimer (md)(2×4), and the $\zeta(4 \times 2)$ reconstructions. Note that the $\text{md}(2 \times 4)$ cell has an As-Ga dimer in the top surface layer and eight Ga atoms in the second layer (see, e.g., Ref. 31). Like for GaAs, the $c(4 \times 4)$ reconstruction was not considered. For these reconstructions all possible N substitutions have been calculated in the first and second anion layers. The thus determined most favorable substitutions are found to be the same as for GaAs(001) surface reconstructions.

The computed stability phase diagrams for InAs(001) are shown in Fig. 8(a) for N in InAs bulk, in Fig. 8(b) [Fig. 8(c)] for the second (first) anion surface layer. Very similar conclusions as for the GaAs(001) surface can be drawn: (i) all surfaces reduce the energy to substitute N, (ii) the second anion layer is energetically more favorable for N than the first, (iii) N exhibits a complex behavior at the surface and affects the stability of the reconstructions, and (iv) finally, a key difference is that the formation energies of N substitutions in InAs are generally higher than those in the corresponding GaAs case. A consequence is that all N substitutions in InAs are thermodynamically not stable.

Contour lines with constant concentration were also calculated (Fig. 8). They were chosen, so that they coincide

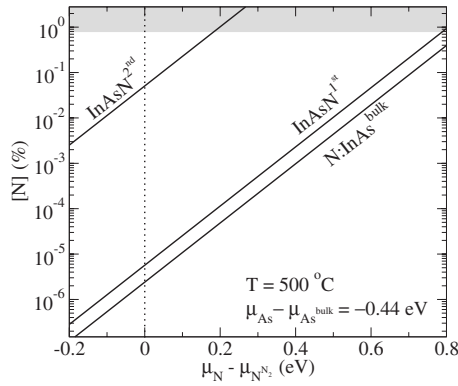


FIG. 9. Calculated N concentration in InAs as a function of N chemical potential at $T=500$ °C and $\mu_{\text{As}} - \mu_{\text{As}^{\text{bulk}}} = -0.44$ eV. Different lines represent the different N incorporation mechanisms.

partially (at the As-rich conditions limit) with the corresponding lines in the GaAsN phase diagrams to allow for a convenient comparison between the two materials.

From the concentration lines a slightly different behavior of N solubility than in the case of GaAs results. The differences are mainly related to the presence of an additional surface reconstruction [$\text{md}(2 \times 4)$] that becomes stable under As-poor conditions. Nevertheless, very similar features as in the case of GaAs are found and can be summarized as follows. (i) The N solubility is strongly affected by surface reconstruction. (ii) The N solubility generally increases with decreasing As chemical potential. The discontinuities occur at phase transitions [here at the $\text{md}(2 \times 4)$ phase]. In contrast to the GaAs case the discontinuity at the boundary does not lead to a reduction in the N solubility when going toward As-poor conditions. (iii) The solubility of N in the subsurface region (second anion layer) is higher by up to 4 orders of magnitude than the solubility at the uppermost surface layer (first anion layer), which is similar to the case of GaAs. (iv) The solubility at the subsurface is higher than that in the bulk by about 3–4 orders of magnitude, while no considerable solubility enhancement can be noticed in the case of the top surface layer. For both surface and subsurface incorporations the optimal As chemical potential (μ_{As}) to achieve a maximal N concentrations is around the region of the phase transition from $\beta 2(2 \times 4)$ to $\alpha 2(2 \times 4)$, i.e., $\mu_{\text{As}} - \mu_{\text{As}^{\text{bulk}}} = -0.44$ eV.

The N solubility as a function of the N chemical potential and at the optimal As chemical potential for the three different N incorporation mechanisms [surface, subsurface, and bulk (equilibrium) incorporation] has been calculated and is shown in Fig. 9. Experimentally, the achieved N concentration in InAs is low and in the range of 0.8%–2.8%.^{11,43–45} However, it is reported that isolated N substitutions are present only for low N concentration (0.5%); at higher concentrations (1.2%) dinitrogen In complexes tend to form.⁴⁶ So far no information is available about the kinetic barriers of N for the subsurface incorporation in the InAs(001) surface. Hence, the operational N incorporation mechanisms cannot be directly determined. Assuming that InAs(001) follows the case of the GaAs(001) surface, i.e., only the first anion surface layer incorporation is possible, the upper limit

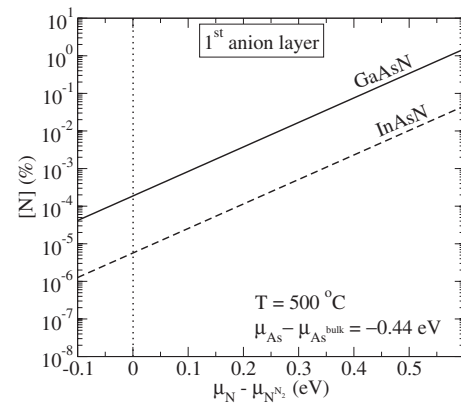


FIG. 10. Comparison of the calculated N concentrations in InAs and GaAs as a function of N chemical potential at $T=500$ °C and $\mu_{\text{As}} - \mu_{\text{As}^{\text{bulk}}} = -0.44$ eV, assuming first layer N incorporation.

of the N chemical potential (μ_{N_2}) should be considered to be higher in practice by ≥ 0.8 eV based on the same arguments discussed in the case of GaAs.

Let us now compare between the solubility of N in InAs and in GaAs. Comparing Figs. 5 and 9 it becomes clear that the N solubility is generally less in InAs than in GaAs. For an incorporation in bulk it is less by about 1 order of magnitude (roughly a factor of 25 times), in the first anion layer by ~ 1 –4 orders of magnitude and in the second anion layer by ~ 1 –2 orders of magnitude. The significant differences have their origin in the interplay between chemical and strain energy; the lattice mismatch between GaAs/GaN is larger than that between InAs/InN while the binding energy of InN is less than that of GaN. The effect of the chemical energy will be pronounced more at the surface layers because of better strain relaxation. For comparison, we show in Fig. 10 the N concentrations resulting from the N solubility in the first anion layer in both GaAs and InAs at $\mu_{\text{As}} - \mu_{\text{As}^{\text{bulk}}} = -0.44$ eV. The figure shows an approximately ~ 30 times lower N concentration at InAs than at GaAs surface at identical μ_{N} . Experimental studies showed that the N content in InAs is systematically lower than in GaAs and that $\text{InAs}_{1-x}\text{N}_x$ alloys exhibit a N concentration which is roughly 25 times smaller than in $\text{GaAs}_{1-x}\text{N}_x$ under identical growth conditions ($T=420$ °C).¹¹ These experimental findings agree well with the results obtained here for the first anion layer incorporation at the optimal μ_{As} .

The results obtained here allow also for some conclusions regarding the growth of quaternary $\text{In}_x\text{Ga}_{1-x}\text{As}_{1-y}\text{N}_y$ alloys. For example, the large difference between the N solubility in InAs and GaAs surfaces indicates that the presence of In on GaAs surfaces will have a large impact on the incorporation or distribution of N. The presence of In on the surface will make it less favorable for N to stick to the surface implying an inverse relation between the N concentration and the In concentration (i.e., the N concentration decreases with increasing In concentration). This situation is very different from the simple bulk thermodynamics picture according to which the addition of In should enhance the N solubility. Also, the N adatoms will bind preferably with Ga rather than with In indicating an In-N anticorrelation in $\text{In}_x\text{Ga}_{1-x}\text{As}_{1-y}\text{N}_y$ alloys which indeed has been observed.¹⁵

IV. CONCLUSIONS

Based on an extensive DFT study on the incorporation of N at the surface, in the subsurface and in the bulk of GaAs and InAs we were able to determine solubility limits for various incorporation mechanisms. Our results show that the solubility of N at and in surfaces is a complex function of growth conditions and depends strongly on the specific surface reconstruction and layer. The solubility of N is found to be highest at the subsurface for all considered surface reconstructions. However, a careful analysis showed that N incorporation is restricted to the first surface layer. An equilibration of N in the deep layers or bulk with the top surface layer is kinetically suppressed. The N bulk concentration is therefore solely dictated by the N solubility of the first surface layer. Our results show further that the high N concentrations

achieved in experiment can be only explained by growth conditions far away from thermodynamic equilibrium. The N atoms at the surface do not equilibrate with an N₂ gas, as assumed in previous theoretical studies but with a gas of activated N₂ molecules as characteristic for the experimentally used N-plasma sources. Finally, a comparison of N incorporation at GaAs and InAs surfaces shows that the latter has a significantly lower solubility by 1–4 orders of magnitude.

ACKNOWLEDGMENTS

We thank the Deutsche Forschungsgemeinschaft for the financial support under Contract No. NE428/7-2 and Martin Albrecht for fruitful discussions.

-
- ¹M. Weyers, M. Sato, and H. Ando, *Jpn. J. Appl. Phys., Part 2* **31**, L853 (1992).
- ²J. Neugebauer and C. G. Van de Walle, *Phys. Rev. B* **51**, 10568 (1995).
- ³S.-H. Wei and A. Zunger, *Phys. Rev. Lett.* **76**, 664 (1996).
- ⁴I. hsiu Ho and G. Stringfellow, *J. Cryst. Growth* **178**, 1 (1997).
- ⁵J. Tersoff, *Phys. Rev. Lett.* **74**, 5080 (1995).
- ⁶S. B. Zhang and A. Zunger, *Appl. Phys. Lett.* **71**, 677 (1997).
- ⁷M. Kondow, K. Uomi, A. Niwa, T. Kitatani, S. Watahiki, and Y. Yazawa, *Jpn. J. Appl. Phys., Part 1* **35**, 1273 (1996).
- ⁸S. R. Kurtz, A. A. Allerman, E. D. Jones, J. M. Gee, J. J. Banas, and B. E. Hammons, *Appl. Phys. Lett.* **74**, 729 (1999).
- ⁹K. Volz, D. Lackner, I. Nemeth, B. Kunert, W. Stolz, C. Baur, F. Dimroth, and A. W. Bett, *J. Cryst. Growth* **310**, 2222 (2008).
- ¹⁰D. K. Shih, H. H. Lin, and Y. H. Lin, *Electron. Lett.* **37**, 1342 (2001).
- ¹¹V. Sallet, L. Largeau, O. Mauguin, L. Travers, and J. C. Harmand, *Phys. Status Solidi B* **242**, R43 (2005).
- ¹²J.-M. Chauveau, A. Trampert, K. H. Ploog, and E. Tournie, *Appl. Phys. Lett.* **84**, 2503 (2004).
- ¹³X. Kong, A. Trampert, E. Tourmié, and K. H. Ploog, *Appl. Phys. Lett.* **87**, 171901 (2005).
- ¹⁴D. Litvinov, D. Gerthsen, A. Rosenauer, M. Hetterich, A. Grau, P. Gilet, and L. Grenouillet, *Appl. Phys. Lett.* **85**, 3743 (2004).
- ¹⁵M. Albrecht, H. Abu-Farsakh, T. Remmele, I. Hausler, L. Geelhaar, H. Riechert, R. Fornari, and J. Neugebauer, *Phys. Rev. Lett.* **99**, 206103 (2007).
- ¹⁶www.sphinxlib.de
- ¹⁷J. P. Perdew, K. Burke, and M. Ernzerhof, *Phys. Rev. Lett.* **77**, 3865 (1996).
- ¹⁸L. Kleinman and D. M. Bylander, *Phys. Rev. Lett.* **48**, 1425 (1982).
- ¹⁹N. Troullier and J. L. Martins, *Phys. Rev. B* **43**, 1993 (1991).
- ²⁰H. J. Monkhorst and J. D. Pack, *Phys. Rev. B* **13**, 5188 (1976).
- ²¹W. A. Harrison, *Electronic Structure and the Properties of Solids* (Dover, New York, 1989).
- ²²The error is larger for some high-energy substitutional sites (the largest error is 0.23 eV). Nevertheless this does not affect the calculation of N solubility since due to their high energy the occupation of these sites at realistic growth conditions turns out to be negligible.
- ²³*CRC Handbook Of Chemistry and Physics*, 86th ed., edited by D. R. Lide (CRC, Boca Raton, FL, 2005).
- ²⁴M. Fuchs, J. L. F. Da Silva, C. Stampfl, J. Neugebauer, and M. Scheffler, *Phys. Rev. B* **65**, 245212 (2002).
- ²⁵M. R. Ranade, F. Tessier, A. Navrotsky, and R. Marchand, *J. Mater. Res.* **16**, 2824 (2001).
- ²⁶P. Laukkanen *et al.*, *Phys. Rev. Lett.* **100**, 086101 (2008).
- ²⁷P. Laukkanen, M. Ahola-Tuomi, M. Kuzmin, R. E. Perala, I. J. Vayrynen, A. Tukiainen, J. Pakarinen, M. Saarinen, and M. Pessa, *Appl. Phys. Lett.* **90**, 082101 (2007).
- ²⁸S. Z. Wang, S. F. Yoon, and W. K. Loke, *J. Appl. Phys.* **94**, 2662 (2003).
- ²⁹A. R. Kovsh, J. S. Wang, L. Wei, R. S. Shiao, J. Y. Chi, B. V. Volovik, A. F. Tsatsul'nikov, and V. M. Ustinov, *J. Vac. Sci. Technol. B* **20**, 1158 (2002).
- ³⁰S. H. Lee, W. Moritz, and M. Scheffler, *Phys. Rev. Lett.* **85**, 3890 (2000).
- ³¹W. G. Schmidt, *Appl. Phys. A: Mater. Sci. Process.* **75**, 89 (2002).
- ³²A. Jenichen, C. Engler, G. Leibiger, and V. Gottschalch, *Phys. Status Solidi B* **242**, 2820 (2005).
- ³³S. B. Zhang and S.-H. Wei, *Phys. Rev. Lett.* **86**, 1789 (2001).
- ³⁴T. Hashizume, Q. K. Xue, J. Zhou, A. Ichimiya, and T. Sakurai, *Phys. Rev. Lett.* **73**, 2208 (1994).
- ³⁵R. Z. Bakhtizin, T. Sakurai, Q. K. Xue, and T. Hashizume, *Phys. Usp.* **167**, 1227 (1997).
- ³⁶W. G. Schmidt, *Appl. Phys. A: Mater. Sci. Process.* **65**, 581 (1997).
- ³⁷M. Itoh and T. Ohno, *Phys. Rev. B* **62**, 7219 (2000).
- ³⁸H. Abu-Farsakh and J. Neugebauer (unpublished).
- ³⁹J. S. Wang, A. R. Kovsh, L. Wei, J. Y. Chi, Y. T. Wu, P. Y. Wang, and V. M. Ustinov, *Nanotechnology* **12**, 430 (2001).
- ⁴⁰Q. X. Zhao, S. M. Wang, M. Sadeghi, A. Larsson, M. Friesel, and M. Willander, *Appl. Phys. Lett.* **89**, 031907 (2006).
- ⁴¹W. G. Bi and C. W. Tu, *Appl. Phys. Lett.* **70**, 1608 (1997).
- ⁴²H. Carrere, A. Arnoult, A. Ricard, X. Marie, T. Amand, and E. Bedel-Pereira, *Solid-State Electron.* **47**, 419 (2003).
- ⁴³T. D. Veal, L. F. J. Piper, P. H. Jefferson, I. Mahboob, C. F.

- McConville, M. Merrick, T. J. C. Hosea, B. N. Murdin, and M. Hopkinson, *Appl. Phys. Lett.* **87**, 182114 (2005).
- ⁴⁴S. Nishio, A. Nishikawa, R. Katayama, K. Onabe, and Y. Shiraki, *J. Cryst. Growth* **251**, 422 (2003).
- ⁴⁵Q. Zhuang, A. Godenir, and A. Krier, *J. Phys. D* **41**, 132002 (2008).
- ⁴⁶J. Wagner, K. Kohler, P. Ganser, and M. Maier, *Appl. Phys. Lett.* **87**, 051913 (2005).